

TECHNICAL REPORT BRL-TR-3047

BRL

AD-A213 327

THE EFFECT OF SABOT FRONT BORERIDER STIFFNESS
ON THE LAUNCH DYNAMICS OF FIN-STABILIZED
KINETIC ENERGY AMMUNITION

PETER PLOSTINS
ILMARS CELMINS
JONATHAN BORNSTEIN
J. E. DIEBLER, BATTIELLE PACIFIC

DTIC
ELECTE
OCT. 12 1989
S B D

OCTOBER 1989

APPROVED FOR PUBLIC RELEASE; DISTRIBUTION UNLIMITED.

U.S. ARMY LABORATORY COMMAND

BALLISTIC RESEARCH LABORATORY
ABERDEEN PROVING GROUND, MARYLAND

89 10 12 03 T

DESTRUCTION NOTICE

Destroy this report when it is no longer needed. DO NOT return it to the originator.

Additional copies of this report may be obtained from the National Technical Information Service, U.S. Department of Commerce, Springfield, VA 22161.

The findings of this report are not to be construed as an official Department of the Army position, unless so designated by other authorized documents.

The use of trade names or manufacturers' names in this report does not constitute indorsement of any commercial product.

UNCLASSIFIED

SECURITY CLASSIFICATION OF THIS PAGE

REPORT DOCUMENTATION PAGE

Form Approved
OMB No. 0704-0188

1a. REPORT SECURITY CLASSIFICATION UNCLASSIFIED		1b. RESTRICTIVE MARKINGS	
2a. SECURITY CLASSIFICATION AUTHORITY		3. DISTRIBUTION / AVAILABILITY OF REPORT Approved for public release; distribution unlimited.	
2b. DECLASSIFICATION / DOWNGRADING SCHEDULE		4. PERFORMING ORGANIZATION REPORT NUMBER(S) BRL-TR-3047	
4. PERFORMING ORGANIZATION REPORT NUMBER(S) BRL-TR-3047		5. MONITORING ORGANIZATION REPORT NUMBER(S)	
6a. NAME OF PERFORMING ORGANIZATION U.S. Army Ballistic Research Laboratory	6b. OFFICE SYMBOL (If applicable) SLCBR-LF-D	7a. NAME OF MONITORING ORGANIZATION	
6c. ADDRESS (City, State, and ZIP Code) Aberdeen Proving Ground, MD 21005-5066		7b. ADDRESS (City, State, and ZIP Code)	
8a. NAME OF FUNDING / SPONSORING ORGANIZATION U.S. Army Ballistic Research Laboratory	8b. OFFICE SYMBOL (If applicable) SLCBR-DD	9. PROCUREMENT INSTRUMENT IDENTIFICATION NUMBER	
8c. ADDRESS (City, State, and ZIP Code) Aberdeen Proving Ground, MD 21005-5066		10. SOURCE OF FUNDING NUMBERS	
		PROGRAM ELEMENT NO. 62618	PROJECT NO. 1L1 62618AH80
		TASK NO.	WORK UNIT ACCESSION NO.
11. TITLE (Include Security Classification) THE EFFECT OF SABOT FRONT BORERIDER STIFFNESS ON THE LAUNCH DYNAMICS OF FIN-STABILIZED KINETIC ENERGY AMMUNITION			
12. PERSONAL AUTHOR(S) Plostins, Peter, Celmins, Ilmars, and Bornstein, Jonathan, and Diebler, J.E.*			
13a. TYPE OF REPORT Technical Report	13b. TIME COVERED FROM _____ TO _____	14. DATE OF REPORT (Year, Month, Day) 1989 July 27	15. PAGE COUNT 38
16. SUPPLEMENTARY NOTATION *Mr. Diebler - Battelle Pacific Northwest Laboratory, Richland, WA			
17. COSATI CODES		18. SUBJECT TERMS (Continue on reverse if necessary and identify by block number)	
FIELD	GROUP	SUB-GROUP	
19	01	Sabot Petal Stiffness,	
19	06	In-Bore Balloting Motion, Interior Ballistics, Gun Tubes, (AIM)	
19. ABSTRACT (Continue on reverse if necessary and identify by block number) The influence of sabot front borerider stiffness on the launch dynamics of generic 25mm fin-stabilized kinetic energy ammunition has been experimentally examined. The effects of this parameter on the jump and dispersion of the ammunition are presented and analyzed. The major conclusions of this report are that: (1) the linear and angular dynamic state of the projectile at shot exit is not dominated by the motion of the gun muzzle but is primarily dependent on the relative motion of the projectile to the bore centerline (i.e., the in-bore balloting), (2) the front borerider stiffness clearly alters the inbore response of the projectile and (3) the dispersion of the ammunition is a result of a complex interaction determined by the dynamic state of the projectile at muzzle exit. <i>Keywords!</i>			
20. DISTRIBUTION / AVAILABILITY OF ABSTRACT <input type="checkbox"/> UNCLASSIFIED/UNLIMITED <input checked="" type="checkbox"/> SAME AS RPT. <input type="checkbox"/> DTIC USERS		21. ABSTRACT SECURITY CLASSIFICATION UNCLASSIFIED	
22a. NAME OF RESPONSIBLE INDIVIDUAL Dr. Peter Plostins		22b. TELEPHONE (Include Area Code) 301-278-3786	22c. OFFICE SYMBOL SLCBR-LF-F

Acknowledgments

The authors wish to express their appreciation to Mr. Donald McClellan, Mr. William Thompson and Mr. John Carnahan for their efforts during the experimental phase of this study.

Accession For	
NTIS GRA&I	<input checked="" type="checkbox"/>
DTIC TAB	<input type="checkbox"/>
Unannounced	<input type="checkbox"/>
Justification	
By	
Distribution/	
Availability Codes	
Dist	Avail and/or Special
A-1	



Table of Contents

	<u>Page</u>
List of Figures	vii
List of Tables	ix
I. Introduction	1
II. Sabot Petal Stiffness Analysis	2
III. Test Instrumentation and Procedure	2
IV. Jump and Dispersion Model	3
V. Presentation and Analysis of the Data	5
VI. Summary and Discussion of the Results	6
VII. Influence of In-bore Balloting Motion	9
VIII. Conclusions	12
References	26
Distribution List	29

List of Figures

<u>Figure</u>		<u>Page</u>
1	Baseline Projectile Assembly	13
2	Photograph of Stiff, Soft and Baseline Scoops	13
3	Stiff Scoop Displacement	13
4	Schematic of Test Set-Up	14
5	Photograph of Test Set-Up	14
6	Close-Up of the Proximity Gauges	14
7	X-ray of the Projectile at 0.11 meter	15
8	X-ray of the Projectile at 2.10 meters	15
9	Jump Model	15
10	Dispersion Model	15
11	Muzzle Displacement	16
12	Muzzle Pointing Angle	16
13	Horizontal C.G. Trajectory of Projectile	16
14	Vertical C.G. Trajectory of Projectile	16
15	Horizontal Yawing Motion	17
16	Vertical Yawing Motion	17
17	Free Flight Motion	17
18	Jump Closure No. 19160	17
19	Muzzle Pointing Angle Summary	18
20	Muzzle Crossing Velocity Summary	18
21	Projectile CG Jump Summary	18
22	Aerodynamic Jump Summary	18
23	Projectile Angular Rate at the Muzzle	19
24	Gun Muzzle Angular Rate	19
25	Cross Correlations for the Soft Configuration	19
26	Cross Correlations for the Stiff Configuration	19
27	Jump Correlation Effect Schematic	20

28	Geometry for the problem of a rigid beam supported by four springs	20
29	Linear displacement of rod center of gravity when traversing a guntube with a sinusoidal bore centerline	21
30	Bore centerline profile for 25mm Mann barrel used in the test	21
31	Linear velocity of the rod center of gravity perpendicular to the centerline of the gun tube	22
32	Angular rate of the rod	22
33	Correlation between aerodynamic and linear jump at the muzzle, in the vertical plane	23
34	Correlation between aerodynamic and linear jump at the muzzle for a ro- tating coordinate system	23

List of Tables

<u>Table</u>		<u>Page</u>
1	Front Borerider Stiffness	24
2	Measured Target Impact Dispersion	24
3	Mean Impact and Dispersion Summary - Baseline Configuration	24
4	Mean Impact and Dispersion Summary - Stiff Configuration	24
5	Mean Impact and Dispersion Summary - Soft Configuration	25
6	Dispersion Results with Jump Correlation Terms	25

I. Introduction

Inbore launch disturbances determine the initial dynamic state imposed on the transitional ballistic phase of projectile launch. During inbore travel, the projectile must traverse a path determined by the static, dynamic and gravity induced curvature of the gun tube. The gravity induced curvature is simply the droop of the gun due to the force of gravity acting on the tube. The static curvature is the bore straightness profile resulting from the inability of the manufacturing processes to machine a perfectly straight tube. The dynamic curvature of the gun tube is a result of complex interdependent events. Part of the dynamic curvature or bending of the gun tube arises from the forces and moments created as the propellant gas pressure acts on the breech. The recoil axis, the mass center of the recoiling parts and the center of rotation are not colinear. Therefore, the propellant gas force causes linear and angular rigid body motion as well as vibrational bending of the gun tube. As this occurs, the propellant gas is also accelerating the projectile along the bore. The projectile responds to the motion of the gun tube walls and the gun tube to a lesser extent responds to the motion of the projectile. This path can be thought of as the forcing function causing the balloting motion of an elastic sub-projectile supported by a group of elastic sabot petals.

The response of the sabot petals to this forcing function determines the linear and angular dynamic state of the sabot/projectile at muzzle exit. The interaction between the sabot boreriders and the tube walls will therefore determine not only the quality of the dynamic state at the muzzle but the level of asymmetry imparted to the projectile. The rear borerider is the stiffer of the two boreriders and can be expected to act more as a pivot point. The front borerider is generally located on the sabot cup and will probably drive the elastic response of the sabot/projectile. The primary objective of the study is to determine how the borerider stiffness affects the launch dynamics and dispersion of the projectile.

Generic 25mm sabot launched fin-stabilized kinetic energy ammunition was tested with sabots whose front borerider stiffness was increased and decreased from that of a baseline configuration. The stiffness of the borerider was computed by an ANSYS finite element analysis, performed under contract by Battelle Pacific Northwest Laboratories. The projectiles were manufactured with 4-petal sabot segments and a steel sub-projectile, Figure (1). A steel sub-projectile was chosen because it has low inertia. Consequently, the sabot/sub-projectile weight ratio is high and any inbore or transitional ballistic disturbances to the sub-projectile are amplified, simplifying measurement.

All aspects of the launch dynamics were measured. These included gun dynamics, transitional ballistics and free flight characteristics. Proximity probes were used to measure the motion of the gun tube muzzle during the inbore cycle and to determine the muzzle pointing angle, linear crossing velocity and angular velocity at shot exit. Six orthogonal flash x-rays recorded the dynamic state of the projectile at the muzzle and subsequent to the sabot discard. The Aerodynamic Range Facility photographed the free flight motion for a distance of 70 meters, thus establishing the projectile trajectory and aerodynamic jump.

II. Sabot Petal Stiffness Analysis

Determining the effective borerider stiffness is a difficult problem. In general, experimental methods clamp either the bulkhead or the saddle of the sabot and apply a force to the sabot scoop and measure the resultant scoop deflection. A load-deflection curve can then be generated for the scoop. This technique has the obvious problem of only measuring the stiffness of one petal. Also, clamping the bulkhead or the saddle will result in different effective stiffnesses. Fixing the bulkhead results in a lower stiffness because the saddle region bends outward under the action of the applied load. An argument can be made for clamping the bulkhead only and including the saddle deflection because the sub-projectile is an elastic member. Another unknown is how and where on the bourellet the force actually acts. One can postulate that as the scoop deflects, the application point of the force moves rearward and the effective stiffness could increase due to the shorter moment arm. The effects of clearances between the sabot and gun tube could result in a load being applied on only one side of the scoop at a given instant. The number of sabot petals is an important parameter to consider. The interface boundary conditions between the petals and the sub-projectile will be affected by the number of petals and must result in a different overall stiffness. A four petal sabot was picked for this study since it has a lower inbore stiffness than a two or three petal system and should amplify the disturbances.

To compare the effects of different scoop stiffnesses, an analytic experiment was conducted to compute a representative front borerider stiffness. An ANSYS finite element code was used to compute the force required for a uniform lateral displacement of a 3-D model of one sabot petal. Penetrator bending was not considered and the boundary condition of a clamped saddle was used. Three sabot petals were analyzed: a baseline scoop configuration, a stiffer scoop and a softer scoop. Figure (2) is a photograph of two baseline sabot/penetrator assemblies, each one next to a stiff and a soft scoop assembly respectively. The different thicknesses of the scoops is clearly visible. Figure (3) shows the displacement of the stiff scoop relative to the undeformed state. Table (1) lists the force to deflection ratio for each sabot petal. This is an effective spring constant representing the different scoop stiffness levels. The percent change in the stiffness from that of the baseline is also listed. Only a 29% reduction in stiffness could be achieved for the soft configuration because the sabot/penetrator assembly would lose its inbore structural integrity if the borerider were weakened any further. These designs were manufactured and tested in the second part of this study.

III. Test Instrumentation and Procedure

A schematic of the test set-up is given in Figure (4). Figure (5) is a photograph of the set-up and Figure (6) is a closeup of the proximity gage arrangement at the muzzle. The dynamic state of the muzzle was measured by two stations of proximity probes located 10.7 cm and 20.8 cm from the muzzle of the gun. At each station, four Scientific-Atlanta model 61 eddy current proximity probes were mounted in protective plastic holders, with two probes diametrically opposite each other in the horizontal and vertical planes respectively.

A piezoelectric pressure gage shown in Figure (6), placed close to the muzzle provided an instrumentation trigger signal. Using a custom built trigger signal processor that sensed both the precursor shock and the main blast wave, all instrumentation was triggered by the main blast wave pressure pulse. All proximity probe signals were recorded on Nicolet model 4094 digital oscilloscopes at a sampling frequency of 200 KHz. Muzzle displacement, pointing angle, transverse linear velocity and angular velocity were determined utilizing appropriate data reduction techniques. The details of the experimental technique and analysis procedure are given in Reference (1).

A 25mm Mann barrel was used to launch the projectiles at a nominal velocity of 1525 m/s. Seven baseline and one five round group each of the stiffer and softer scoop configurations were launched. The transitional ballistics of the projectiles were measured following the procedures outlined in References (2) and (3). Six orthogonal x-ray stations at the muzzle, nominally located 0.11, 0.45, 0.82, 1.33, 1.71 and 2.10 meters from the muzzle recorded the dynamics of the projectile at muzzle exit. Figures (7) and (8) are horizontal x-ray images of the baseline configuration at 0.11 and 2.10 meters respectively. The photographs indicate that the sabot petals are still in aerodynamic contact with the sub-projectile 2.10 meters downrange.

The fiducial cable used to measure the projectile orientation and position can also be seen in the x-ray images. The test procedure required suspending the cable on the line of fire through the center of the muzzle and the first group of Aerodynamic Range stations. A low level x-ray of the cable was taken as well as photographs of cable fiducial beads at each range station. From the range photographs, the fiducial cable can be located in the range coordinate system; therefore, the location of the beads under each x-ray head are known. The precise location of the muzzle could also be determined from the fiducial cable. The cable was then removed and a second x-ray image of the projectile is recorded on the film during the test. The result is the double image presented in the xray photographs above. This technique was also used in Reference (3).

A target was located in the last station of the third or fourth group of range stations, at 51 or 70 meters respectively. A collimated muzzle borescope was used to locate the target on the line of fire and a nail placed at the aimpoint on the target was photographed in the range station. The coordinates of the muzzle and the target aimpoint were used to determine the pre-shot line of fire.

Using the data reduction procedures and theory documented in Reference (4), a complete set of aerodynamic coefficients were obtained for the sub-projectile, permitting the determination of the aerodynamic jump.

IV. Jump and Dispersion Model

The previously described test set-up and data acquisition procedures are all designed to measure the primary factors contributing to the fall of shot on the target. An early report by Gay and Elder, Reference (5), is an analytic and experimental study of the jump of a 90mm cannon. Only the gun dynamics, the aerodynamic jump and inbore projectile

asymmetries were considered at that time. The authors concluded that these three effects could not account for the jump on the target. A recent paper by Biele, Reference (6), does discuss the sabot separation effects on the jump. Reference (6) concludes that the jump is a vector sum of a series of components and that the gun dynamics alone is not sufficient to close with the target impact.

This paper utilizes the following jump and dispersion models for sabot launched fin-stabilized kinetic energy ammunition. The origin in Figure (9) is the intersection of the target and the pre-shot line-of-fire. An aimpoint can also be defined and is below the origin on the vertical axis. Its magnitude in milliradians is equal to the gravity drop experienced by the projectile at a given range. A jump vector in Figure (9) is a vector, whose horizontal and vertical magnitude is the angle in milliradians of the deviation from the line-of-fire. The jump model for a sabot launched fin-stabilized kinetic energy penetrator consists of the 6 components displayed in Figure (9). The first component is the jump due to muzzle pointing angle. The gun deviates from the line-of-fire prior to shot exit. At shot exit the muzzle of the gun has a transverse velocity which it imposes on the projectile. This determines the second jump component, the muzzle crossing velocity. It is the angle computed by dividing the muzzle transverse velocity by the projectile launch velocity. The third jump component is the angular deviation of the projectile center of gravity from the instantaneous bore centerline at shot exit. This vector is caused by the inbore balloting motion of the projectile, muzzle blast disturbances and projectile mechanical disengagement from the gun tube. The next component is the net deviation of the projectile center of gravity caused by the sabot discard disturbances. The final jump component is the aerodynamic jump or the mean angular deviation of the projectile swerve trajectory. The sixth vector is the gravity drop which is included here for completeness. It is not normally considered a true jump vector but can affect the dispersion if a large variation in projectile muzzle velocity exists. These six jump components are required to determine how the projectile arrived at the target impact point.

Based on the model defining the projectile jump, a dispersion model can be generated. Consider Figure (10); a series of projectiles are fired and a target dispersion is created. This dispersion is the standard deviation of the projectile impacts about the mean impact point. Each impact is created by the sum of a series of different jump components. Each jump component has a dispersion associated with it. Statistically, if the dispersion is the result of the sum of independent events (i.e. the individual jumps), then the square of the standard deviations of the jump components will sum to the square of the impact dispersion. This is true for the horizontal as well as the vertical components. Thus, a dispersion model is described by Equation (1).

$$\sigma^2 = \sigma_{mp}^2 + \sigma_{cv}^2 + \sigma_{cg}^2 + \sigma_{sd}^2 + \sigma_{lj}^2 + \sigma_{gd}^2 \quad (1)$$

It would be simple if the dispersion was a linear sum of the dispersion in six jump components. However, it is possible for the jump components to be interrelated. For instance, it is immediately obvious that the cg jump at the muzzle is coupled to the angular rate of the projectile at the muzzle. Both are determined by the same inbore forcing function. The angular rate at the muzzle, modified by any sabot discard disturbances, is the initial condition for the free flight aerodynamic jump. Therefore in the physical, as well as the statistical sense, a correlation could exist between σ_{cg} and σ_{aj} . This correlation can be

expressed by Equation (2).

$$\sigma_{cga_j} = r\sigma_{c_g}\sigma_{a_j} \quad (2)$$

The factor "r" is a correlation coefficient which can be either positive or negative and is a measure of the statistical strength of the correlation. If such a correlation is found, then Equation (1) must be modified to include this effect. Including the example correlation in Equation (1) results in Equation (3).

$$\sigma^2 = \sigma_{m_p}^2 + \sigma_{c_v}^2 + \sigma_{c_g}^2 + \sigma_{s_d}^2 + \sigma_{a_j}^2 + \sigma_{g_d}^2 + 2\sigma_{cga_j} \quad (3)$$

Correlations can exist between all of the components statistically and the one in Equation (3) has been used as an example of how to include this effect in the sum. Later in the paper, data and physical justifications will be presented as to why this particular correlation was chosen. In the next section the test data will be analyzed based on the simple model discussed in this section.

V. Presentation and Analysis of the Data

For each of the projectiles launched it was necessary to generate a jump component plot such as described in Figure (9). The complete data required to generate the jump plot and the procedure by which this was accomplished will be presented in this section. Figures (11) and (12) are the muzzle displacement and pointing angle history measured by the proximity probe array for a baseline round, number 19160. From this data the muzzle pointing angle, crossing velocity and angular rate of the gun muzzle were computed. The inbore residence time of this projectile is approximately 2 milliseconds. Both the displacement and pointing angle are plotted as functions of time, and 12 milliseconds prior to shot exit both muzzle displacement and movement are observed. These arise from two sources; the first, is that the line of fire is determined with a borescope in the muzzle of the gun. When the borescope is removed, the gun changes its position and angle as measured by the proximity gages used to measure the gun motion. The second is that the gun is fired by pulling a lanyard which can cause gun motion prior to the propellant ignition.

Figures (13) and (14) are x-ray and Aerodynamics Range data of the horizontal and vertical components of the center of gravity trajectory of the projectile near the muzzle. The solid line is the pre-shot line of fire to which the jump is referenced. The next set of data, Figures (15) and (16), is the horizontal and vertical angular motion of the sub-projectile. Both x-ray data and Aerodynamics Range data are again included. The dashed line in these two plots is the non-linear least squares fit of the free flight yawing motion of the projectile. It is clear that there are no measureable sabot discard disturbances such as those reported in Reference (7) which alter the angular rates during the transitional ballistic phase. This leads to the important conclusion that for this sabot/penetrator system the linear and angular dynamics of the projectile at the muzzle are the initial conditions for the free flight motion of the projectile. The free flight angular motion recorded by the Aerodynamics Range and the fit of that data is presented in 3D in Figure (17). The plane of the total yaw can be clearly identified. It is also the plane containing the aerodynamic jump.

The jump plot can now be composed. Since the data indicated that the sabot discard disturbances were effectively zero, the jump model contains only five components. These components are: the muzzle pointing angle, crossing velocity, projectile center of gravity motion at the muzzle, the aerodynamic jump and the gravity drop. The following technique was utilized to close the jump components with the target impact: first, the muzzle pointing angle jump and muzzle crossing velocity jump vectors were constructed from the origin of the jump plot; second, the gravity drop and aerodynamic jump were extrapolated backward from the target impact. The final component, the projectile center of gravity jump at the muzzle, could then be determined by subtracting the other components from the total jump. A check was then made to see if the center of gravity jump component was consistent with the slope of the swerve data recorded by the x-rays at the muzzle, the Aerodynamics Range swerve data and swerve data fit. This is the dashed line labeled "CG JUMP SLOPE" in Figures (13) and (14), respectively. As can be seen the dashed line is tangent to the swerve fit, solid line in the respective figures which is consistent with penetrator free flight motion. The jump closure for round number 19160 is presented in Figure (18). Each round was analyzed by the above technique and a summary of the results for the three different front borerider stiffnesses is presented in the next section.

VI. Summary and Discussion of the Results

There are only seven rounds of data for the baseline configuration and five rounds each for the soft and stiff boreriders, respectively. These are few data on which to base what would be termed statistically significant conclusions. However, even with so few data, insight can be gained about the physics of the stiffness effects on the launch, accuracy and dispersion of this ammunition type. Table (2) is a summary to the target impact dispersion for the three different cases. The data in the table are all in milliradians.

The obvious conclusion to be drawn from this data is that the projectiles fired from the sabots with the stiff borerider appear to have lower dispersion. The proverbial question is "Why?". As was discussed in the previous section, there are only four jump components and the gravity drop required to close with the target impact point. The gravity drop for the 70 meter trajectory is small, its dispersion is negligible and will be ignored. Figures (19), (20), (21) and (22) are summary plots of the individual jump components. Each jump vector is normalized to its own origin; therefore, these are plots of the magnitude and direction of each component. The muzzle pointing angle, Figure (19), appears randomly distributed in the vertical and generally in the positive horizontal direction for all borerider stiffnesses.

Figure (20), the muzzle crossing velocity, is also randomly distributed but is an order of magnitude smaller. The projectile center of gravity jump at the muzzle is random in magnitude but is directed only in the upper half plane. Its magnitude is significant because it is at least one order larger than the muzzle crossing velocity magnitude. It can therefore be concluded that the projectile linear motion at the muzzle is not due to the motion of the muzzle but depends primarily on the motion of the projectile relative to the instantaneous bore centerline. The aerodynamic jump component, Figure (22), appears completely random in magnitude and direction. Since there are no sabot discard

disturbances, the aerodynamic jump is linearly proportional to the angular rate of the projectile at muzzle exit, Figure (23). Comparing Figure (24), the angular rate of the gun muzzle at shot exit, to the data in Figure (23), a similar conclusion can be drawn for the angular dynamics of the projectile as was for the linear dynamics. The angular rate of the gun does not account for the angular motion of the projectile at the muzzle; it is the angular motion of the projectile relative to the bore that dominates by at least one order of magnitude. Another conclusion to be drawn from these data is that the muzzle pointing angle can contribute to the ammunition dispersion but it is not likely that the muzzle crossing velocity contributes significantly.

The plots provide physical insight to the phenomenon. However, there appears to be no clear indication as to why using the stiff borerider sabots result in the lower target impact dispersion. Tables (3), (4) and (5) are a tabular presentation of the data (in milliradians) previously plotted.

The sum of the mean jump of each component in the horizontal and vertical planes for all three configurations closes nicely with the measured mean impact point on the target. The larger difference in the vertical between the sum and the measured terms is the average gravity drop, which has not been included here. The standard and stiff borerider configurations were launched at a 70 meter target and the soft borerider configurations at a 51 meter target. Therefore, the gravity drop is a little smaller in Table (5). The mean of each of the jump components is not significantly different for the three configurations and neither is the dispersion. The dispersion in the aerodynamic jump component of the stiff configuration is smaller on the average but this is not enough to account for the significantly lower target impact dispersion. Much more interesting is the result in the last two columns of the three tables. For the standard configuration, Table (3) the squares of the individual component dispersions add up to the squares of the target impact dispersion. This result indicates that this case can be modeled by the dispersion model given by Equation (1) and the components are independent of each other. Unfortunately, the stiff configuration, which has the lowest dispersion, and the horizontal dispersion component of the soft configuration do not satisfy the simple dispersion model because the sum of the squares of the individual components is much larger than the square of the target impact dispersion. This leads to the conclusion that the dispersion model given by Equations (2) and (3) must be applied in order to explain the lower target impact dispersion.

If there is a perfect correlation between any two jump components, then the correlation coefficient is one. Because of its extremely small magnitude, any correlation between the muzzle crossing velocity component and any other component even for a correlation coefficient of unity would not play a significant role in Equation (3). This is purely a statistical argument to justify dropping any cross terms containing the muzzle crossing velocity. However, a valid physical argument can also be made. Since the projectiles were all fired from a Mann barrel and its inertial mass is so much larger than that of the projectile inbore weight, the interchange of linear and angular momentum between the projectile and the gun tube will affect the gun dynamics only slightly. The primary driver of the gun dynamics in all probability, see Reference (1), is the response of the tube to the breech pressure and the nature of the recoil system. In this specific case, as was demonstrated in Figures (13) and (14), the effect of the lanyard moving the gun also plays a role. The above reason along with the data presented in Figures (20), (21), (23)

and (24), which shows that the linear and angular dynamics of the projectile at shot exit is not driven by the muzzle dynamics, can be used to conclude that the muzzle pointing angle component should not be correlated to any of the other jump components. The only possible correlation that remains is one between the center of gravity jump at the muzzle and the aerodynamic jump. Physically, there must be a coupling between these two quantities because it is the inbore balloting motion that drives the dynamic state of the projectile at muzzle exit. Both the linear velocity and the angular velocity of the projectile are excited by the same interior ballistic forcing functions (i.e. the dynamic and static curvature of the gun tube). Using the jump component data for the horizontal component of the soft configuration, the existence of this correlation can be confirmed. It can be shown that the correlation coefficient in Equation (2) is directly proportional to the slope of a linear fit of any two components of the jump plotted against each other.

Figure (25) is a plot of the muzzle pointing angle versus the aerodynamic jump, the muzzle pointing angle versus the projectile center of gravity jump and the projectile center of gravity jump versus the aerodynamic jump. Clearly, the slope of the data plotted against the muzzle pointing angle is small if not zero. However, there is a clear negative correlation between the projectile center of gravity jump and the aerodynamic jump. Figure (26) is the same plot but for the horizontal component of the stiff configuration. A similar trend is seen in the data but the scatter in the data is much larger. The cross correlation terms, Equation (2), can now be determined from the data in Figures (25) and (26) and the data for the vertical jump components of the stiff configuration. From a basic statistics text, Reference (8), the relation between the slope of the data and the correlation coefficient is:

$$r = \beta \frac{\sigma_{aj}}{\sigma_{cg}} \quad (4)$$

The solid lines in Figures (25) and (26) are least squares fits of the projectile center of gravity component versus the aerodynamic jump component. The results of using the dispersion model given by Equation (3) are given in Table (6).

Clearly, the addition of the correlation term σ_{cga_j} has helped close the difference between the measured target impact dispersion and the dispersion computed using the dispersion model. In the case of the horizontal component of the soft configuration, the closure is remarkable. It is probably just fortuitous that this occurred; however, the closure for both components of the stiff configuration is good by statistical standards for the number of data points available. Using a χ^2 test, it can be shown that the 80% confidence interval on the measured target impact dispersion is $0.23 < \sigma < 0.62$. In Tables (4) and (5) dispersion obtained from the sum of the individual components is just out of this interval. Using the correlation terms brings the computed dispersion much closer and well within this interval. Statistically this means we have closed the dispersion by using the correlation model to within the ability to measure the data. It is felt that the correlation model for the dispersion includes the important terms required to describe the phenomenon.

Since the correlation term does appear to explain the lower dispersion numbers, a physical explanation for the phenomenon is also required. To aid in understanding what is occurring, Figure (27) is helpful. Consider the simple case of only two jump components. In Figure (27) the first jump component is random in magnitude and direction and

the second is less random in direction but still random in magnitude. The dispersion of each component appears high individually but in the last view "Net Jump" the impact dispersion of the sum of the two components is low, demonstrating the existence of the correlation. Because the aerodynamic jump is proportional to the projectile angular rate at the muzzle and the projectile center of gravity jump is actually the linear velocity at the muzzle, both components are coupled in-bore. The fact that they can interact so directly is unique to this test because there were no sabot discard disturbances. In the case of the baseline configuration and the vertical component of the soft configuration, no correlation terms were found. The only plausible explanation for this is that changing the front borerider stiffness has altered the in-bore dynamic response such that the linear and angular motion at the muzzle is in phase, out of phase or between phases in such a manner to cause a symbiotic interaction reducing the dispersion.

VII. Influence of In-bore Balloting Motion

The experimental study has demonstrated that interrelationships between jump components can have a significant impact upon the magnitude of ammunition dispersion. Through statistical arguments, it was shown that the aerodynamic jump was correlated to the linear motion of the projectile at the muzzle, for some test configurations. Since there were no measurable discard disturbances, potential correlations between the linear cg motion, angular rate at the muzzle, cg motion after sabot discard and aerodynamic jump could be eliminated. The angular rate at the muzzle and the aerodynamic jump are therefore linearly related and the correlation between aerodynamic jump and linear cg motion was not obscured.

In the report, it has been further postulated that the in-bore balloting behaviour of the projectile/sabot represents the link joining the linear and angular dynamics of the bullet at the muzzle. Support for this contention can be garnered through a simplified analysis of projectile in-bore motion, illustrating the potential for a correlation between the linear and angular motion of the projectile as it exits the gun tube.

A number of sophisticated models have been developed to examine the details of projectile in-bore motion, including lumped parameter models, References (9) & (10), and finite element models, Reference (11), capable of accurately predicting the flexing of a penetrator subjected to the large lateral accelerations due to projectile balloting motion. Normally, the computational time required to implement a model is directly related to its sophistication and ability to predict the details of in-bore projectile dynamics. In the current study, interest is limited to demonstrating the potential for a correlation between the angular and linear motion of the projectile at the muzzle, rather than accurately predicting the detailed in-bore dynamics. To accomplish this task, a greatly simplified model is utilized. In this model, the projectile/sabot is simulated by a rigid rod supported by four linear springs representing the front borerider and rear obturator band of a sabot projectile. The stiffness of each spring and its placement with respect to the center of gravity of the rod is equal to that of the corresponding sabot element. Passage of the projectile down the bore of the gun tube is simulated by permitting the point of attachment between each of the springs and the supporting tube to translate in the transverse (y)

direction, as shown in Figure (28). To determine the position of the attachment points as a function of time, only the static geometry of the gun tube (i.e. bore centerline and diameter profiles) are considered.

Although the experiments were conducted for a projectile launched from a rifled tube, the model limits itself to the examination of the planar motion for a nonspinning projectile (i.e. a projectile launched from a smoothbore gun). Also, the dynamics of the rod is represented in terms of the linear motion of its center of gravity y_{cg} and the rotation of the rod about this point, α . This motion can be determined from the summation of forces and moments acting upon the cg.

$$\Sigma F = m\ddot{y}_{cg} \quad (5)$$

$$\Sigma M = I\ddot{\alpha} \quad (6)$$

A fourth order Runge-Kutta technique, Reference (12), is utilized to integrate the equations. The excitation or driving function for the system is due to the passage of the rod down a gun tube having curvature and/or a varying diameter resulting in an extension or compression of the springs over and above that due to the free vibration of the rod. The magnitude of this additional extension/compression is obtained by determining the projectile axial position from a match case computed using the IBHVG2 interior ballistics code, Reference (13), then using the measured bore straightness profile and bore diameter to determine the instantaneous displacement of the attachment point for each spring to the outer wall.

Figure (29) depicts the computed linear displacement of the cg for a rod with characteristics similar to the "baseline" case traversing a gun tube having a sinusoidal bore-straightness profile (wavelength = 1.8m) at constant velocity. Note that the cg motion is larger in amplitude and out of phase with the displacement of the wall at the location of the front borerider. It was found that the magnitude of both the linear and angular motion for the projectile/sabot will be a function of the magnitude and frequency of the bore centerline and diameter profiles as well as the placement and stiffness of the supporting springs.

In the model, provision has been made to incorporate the effects of manufacturing tolerances for both the projectile and gun tube through the use of non-linear stiffness functions for the springs (i.e. springs are linear but act only when a sabot element is compressed) and non-zero initial conditions for both the linear and angular position of the rod. The gun tube utilized for the experiment was unusually straight. The measured bore straightness profile, Figure (30), reveals only a few small "bumps" with a magnitude larger than the sensitivity of the measurement technique. In the model, the measured values for bore straightness were used directly with no attempt to pass a smooth curve through the points. The bore curvature will therefore cause a series of impulse disturbances to be applied to the spring-mass system. Since a thick wall Mann Barrel was employed in the tests, the "droop" of the tube is also expected to be small and was not included in the computation. The bore diameter was, except for the zone where rifling begins, uniformly 25.02mm.

For the current analysis, it is assumed that dispersion is due solely to differences in the initial orientation of the projectile in the forcing cone of the gun tube, presumably due to permitted tolerances when the projectile is loaded into the cartridge. Figure (31) depicts the linear rate of the cg perpendicular to the gun tube centerline for six possible initial conditions, with the projectile: (1) cocked upwards to the full extent permitted by the diameter of the gun, (2) parallel to the gun centerline, but placed initially at the bottom of the tube, (3) cocked downwards to the full extent permitted, (4) parallel to the gun centerline with the rod cg at the centerline of the tube, (5) cocked upwards, but only to half the amount permitted by the diameter of the tube and (6) cocked downwards to half the permitted amount. In all cases the diameter of the rod is 25mm.

The results can be placed into two groups. The first, consisting of cases for which the cg was initially below the centerline of the tube exhibits an oscillatory motion with a dominant frequency roughly equal to the natural frequency of the equivalent spring-mass system. The second group was positioned with the cg initially above the centerline of the gun and therefore the rod was not subjected to the same initial disturbance. At the muzzle the motion of the two groups appears to be out of phase due to the different disturbances to which they were exposed.

Figure (32) shows the angular rates (angular velocity multiplied by the forward projectile velocity) for the same six initial conditions. Here a monotonic decrease of the rate at the muzzle can be observed as one proceeds from the cocked up position through the straight initial state to the cocked down position. Plotting the aerodynamic jump versus the linear jump, Figure (33), a negative correlation between the two velocities can be readily observed for the "stiff" case. The figure also depicts results for "baseline" and "soft" boreriders. There are positive correlations for both, approximately 3.4 times larger than the negative correlation for the "stiff" case.

Care must be taken when interpreting the results. As already noted, the balloting motion of the system will be a function of not only the stiffness and position of the supports, but also the geometry of the gun tube (i.e. curvature and variation of diameter along the bore) and the axial acceleration of the projectile in-bore. Therefore, results obtained for this launch system may not be directly applicable to other gun tubes. As an example, a similar computation was conducted for a system, in which the coordinate system was permitted to rotate at an angular rate proportional to the forward velocity of the projectile, modifying the driving function for the system. Figure (34) depicts the relationship between projectile aerodynamic and linear jump in the vertical plane with respect to the gun tube. In this instance, the correlation for the "stiff" borerider has increased in magnitude while remaining negative. The "baseline" and soft borerider results show that the correlations have decreased in magnitude by one-half the value computed for the non-rotating case.

In summary, computations performed utilizing this simplified model have demonstrated that the angular velocity and linear velocity of the projectile at the muzzle can be correlated. The rates will depend upon the projectile properties, the initial conditions, and the in-bore geometry of the launch system and can produce correlations which increase or decrease dispersion. Ideally, one should strive to design a system which is least sensitive to anticipated variations in both the launch system and projectile geometries.

VIII. Conclusions

The purpose of this research was to analyze the effects of structural changes in the sabot components on the launch dynamics, accuracy and dispersion of fin-stabilized kinetic energy ammunition. It had been hoped to find a simple design criterion for improving the performance of the ammunition. Unfortunately, such a rule is not forthcoming. Based on the data, a significant understanding of the factors influencing the accuracy and dispersion of this ammunition type was obtained. The dispersion model proposed by the authors appears adequate to explain the physics of the ammunition dispersion. Because the sabot/penetrator launch system is structurally very elastic, understanding the inbore dynamic response of the projectile is the key to determining the initial conditions which are needed to predict the accuracy and dispersion characteristics of the ammunition.

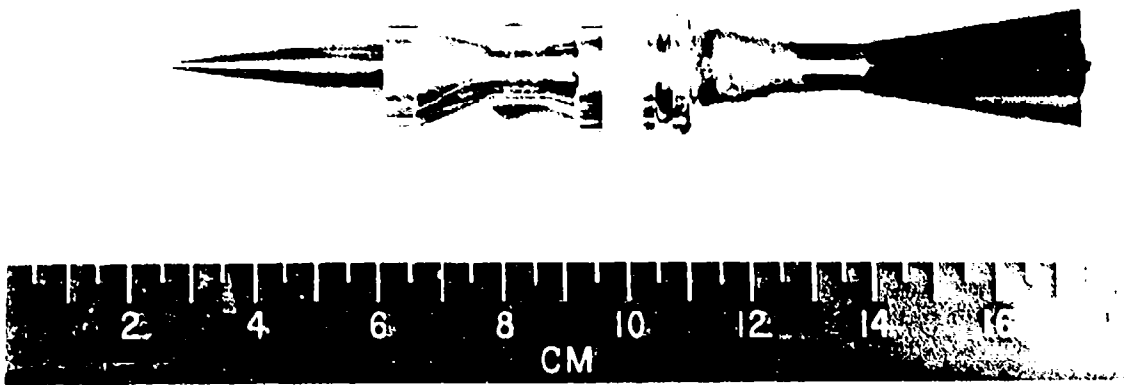


Figure (1) Baseline Projectile Assembly

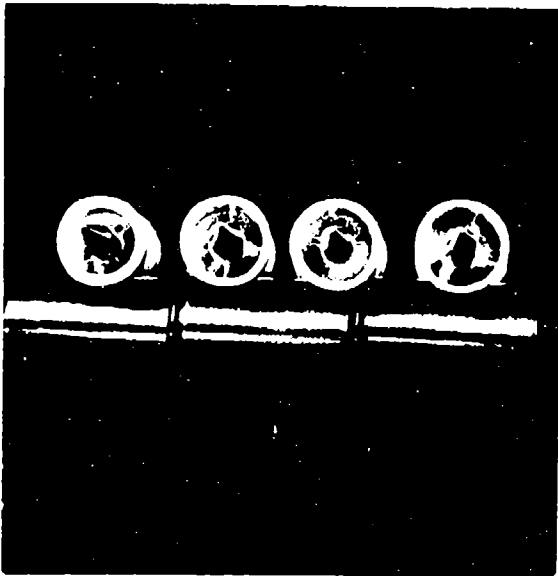


Figure (2) Photograph of Stiff, Soft and Baseline Scoops

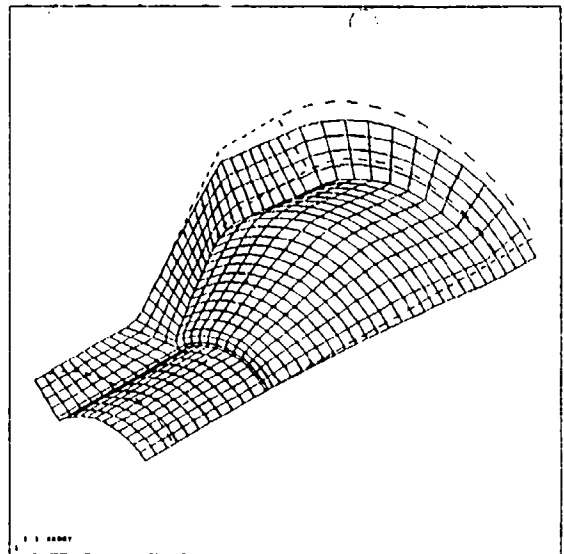


Figure (3) Stiff Scoop Displacement

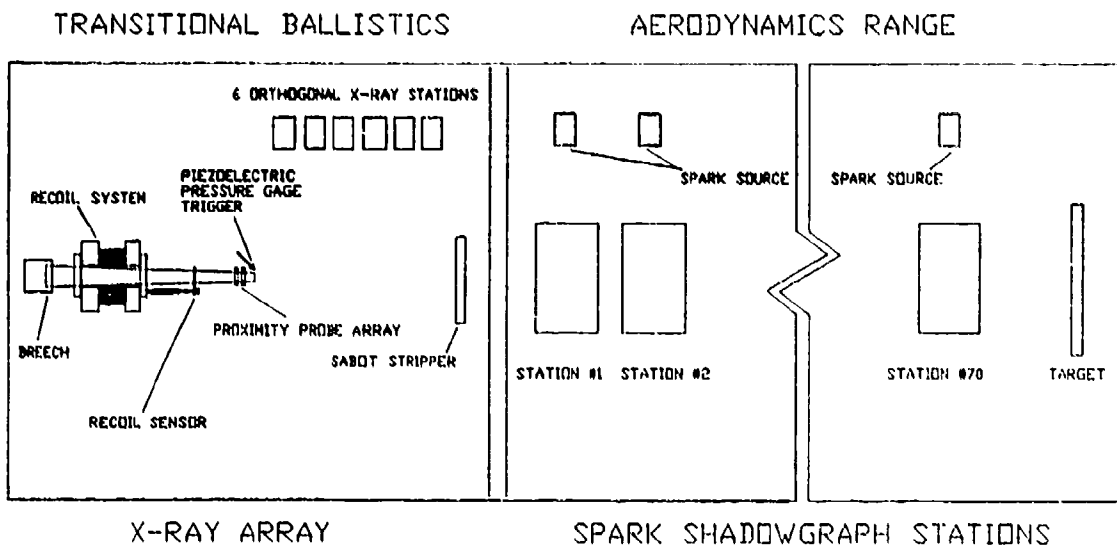


Figure (4) Schematic of the Test Set-Up

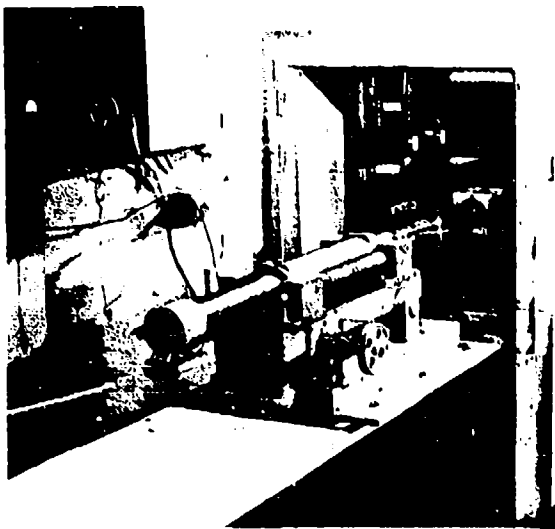


Figure (5) Photograph of Test Set-Up

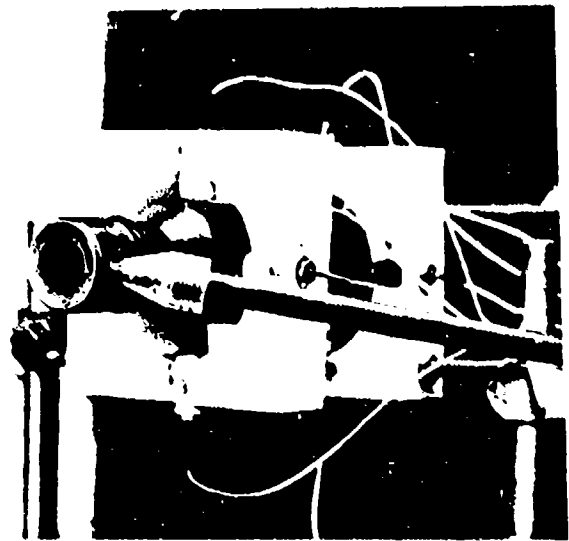


Figure (6) Close-Up of the Proximity Gages

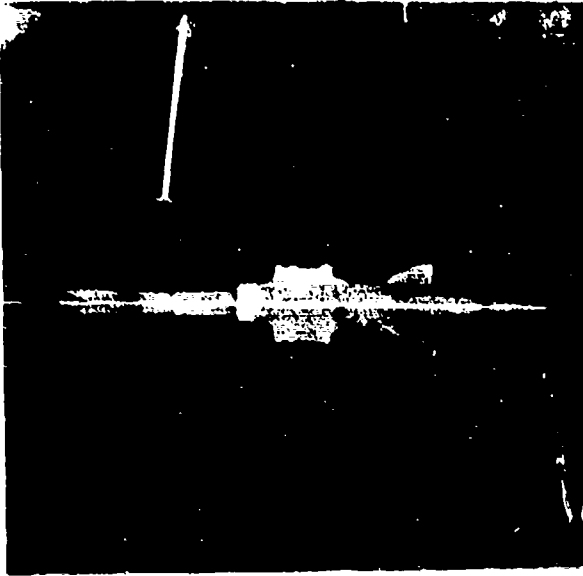


Figure (7) X-Ray of the Projectile at 0.11 meter

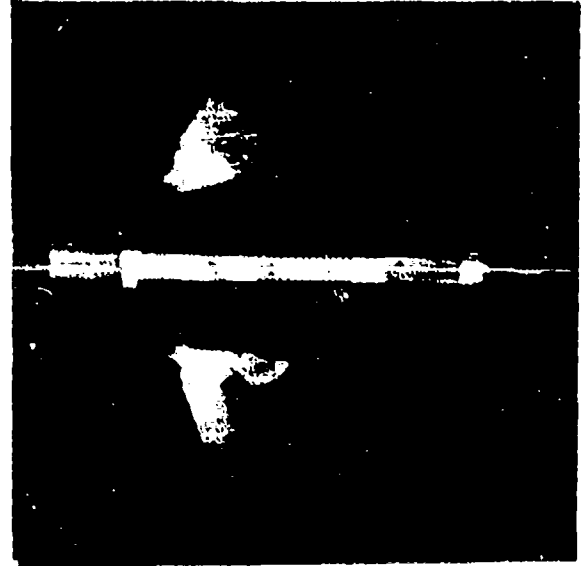


Figure (8) X-Ray of the Projectile at 2.10 meters

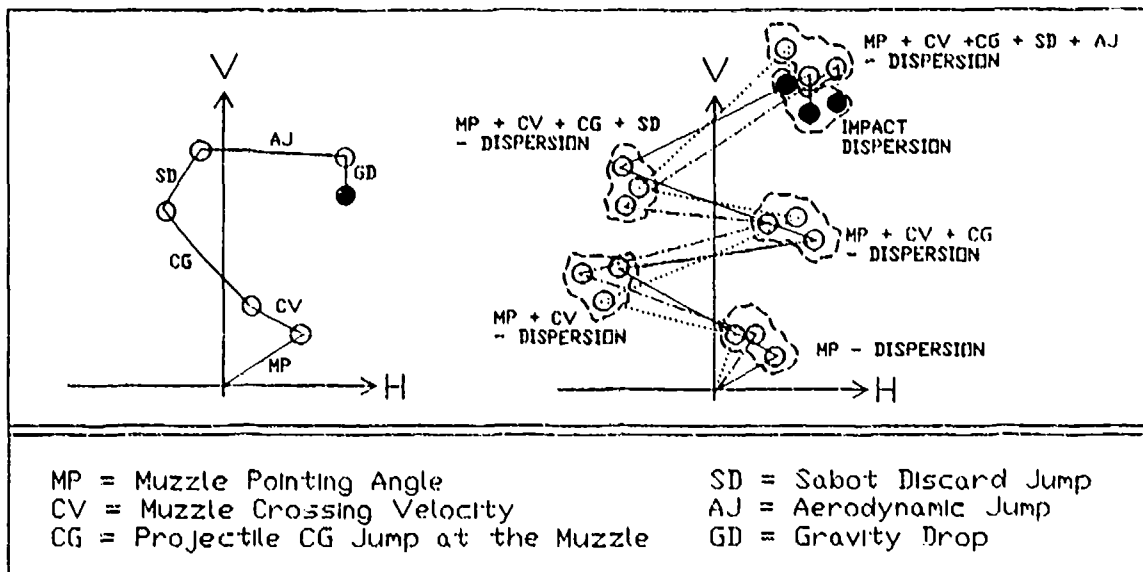


Figure (9) Jump Model

Figure (10) Dispersion Model

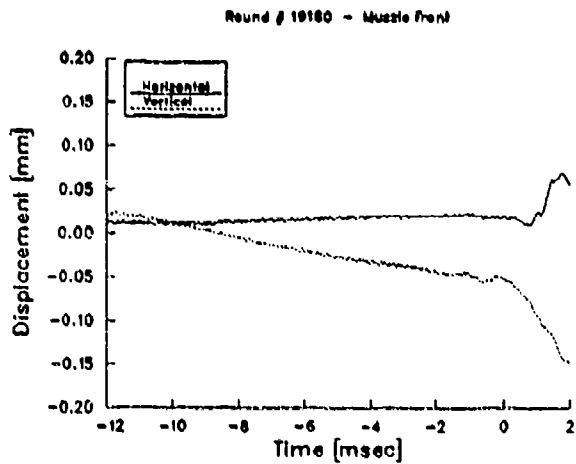


Figure (11) Muzzle Displacement

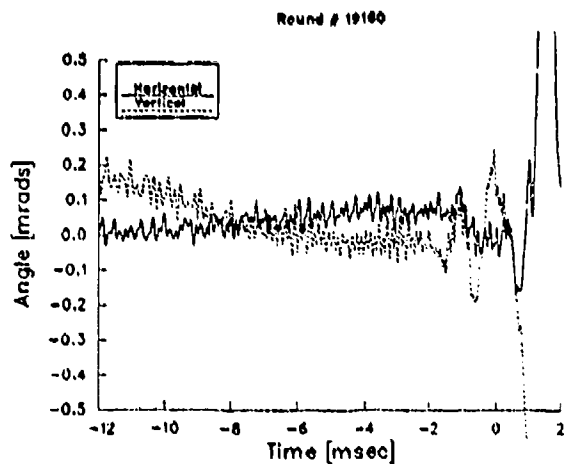


Figure (12) Muzzle Pointing Angle

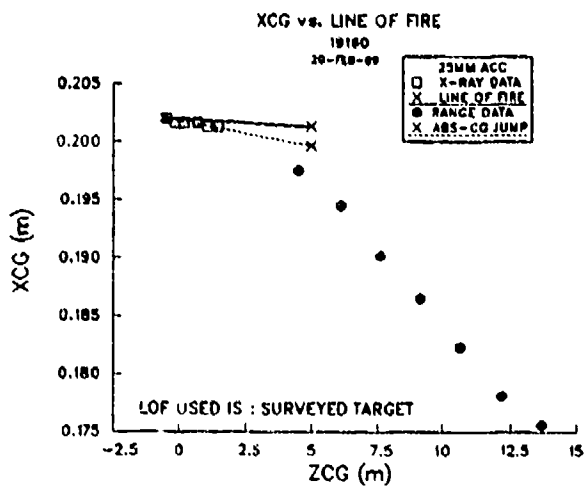


Figure (13) Horizontal C.G. Trajectory of Projectile

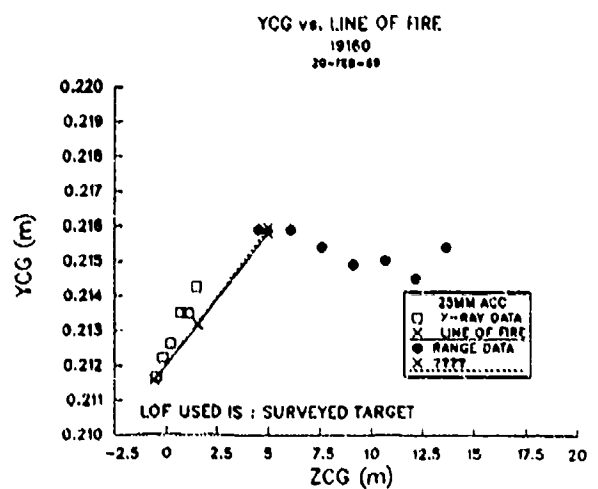


Figure (14) Vertical C.G. Trajectory of Projectile

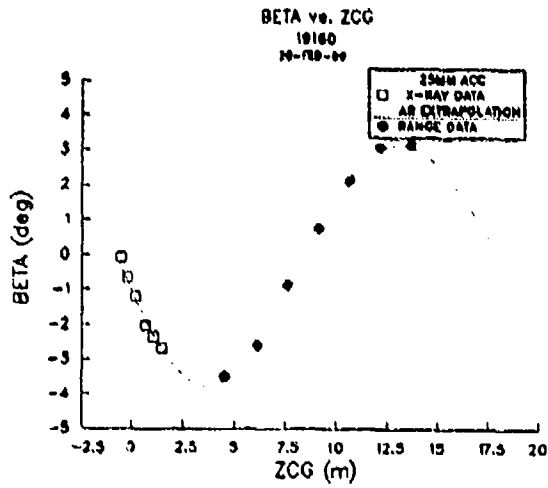


Figure (15) Horizontal Yawing Motion

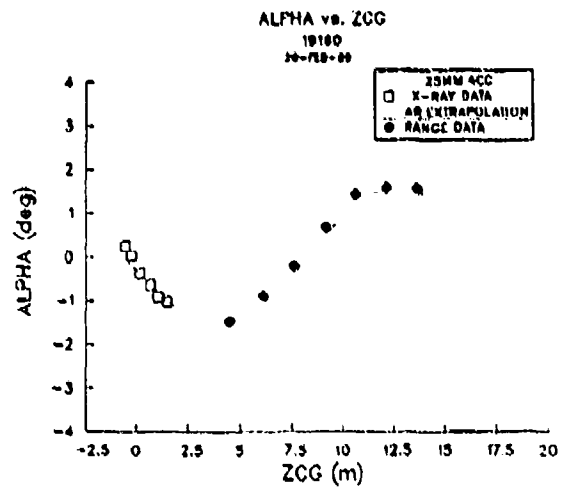


Figure (16) Vertical Yawing Motion

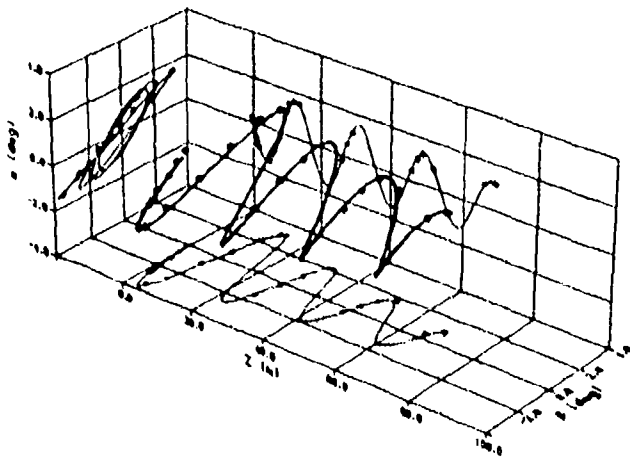


Figure (17) Free Flight Motion

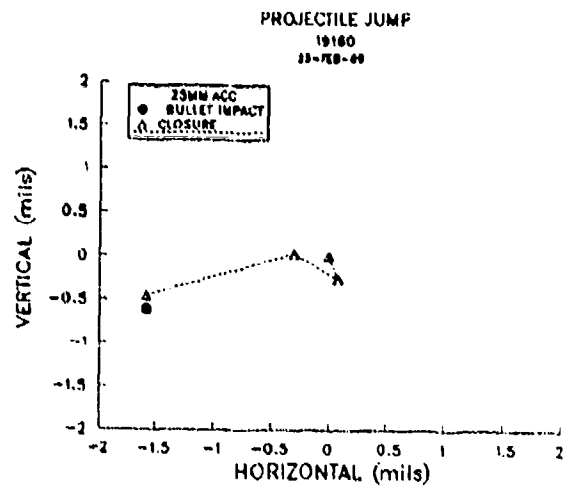


Figure (18) Jump Closure No.19160

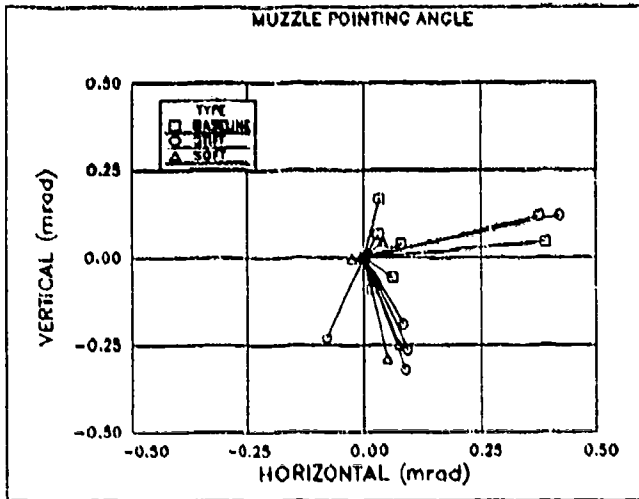


Figure (19) Muzzle Pointing Angle Summary

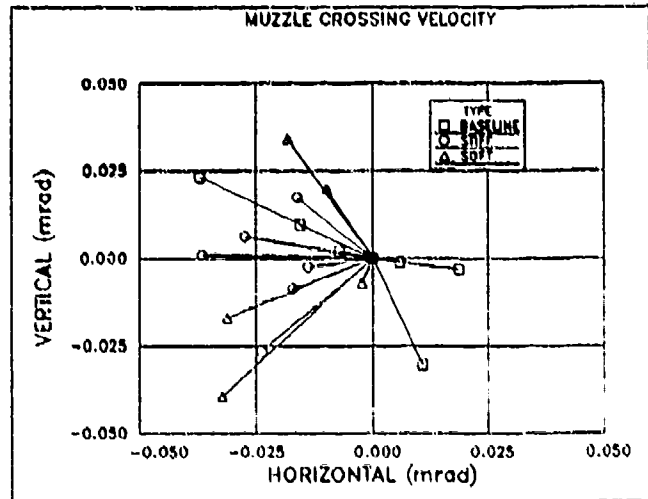


Figure (20) Muzzle Crossing Velocity Summary

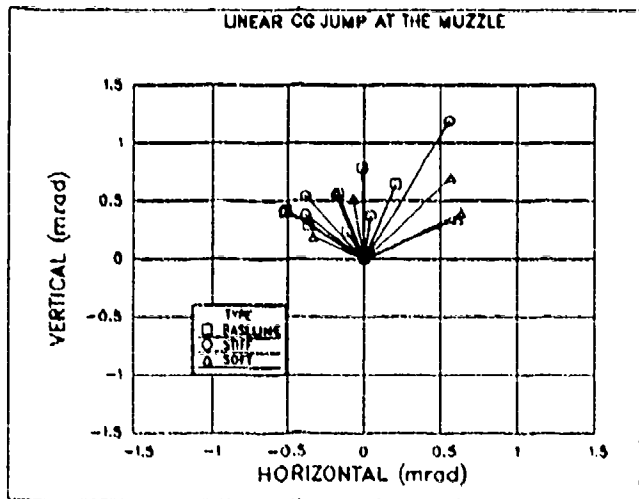


Figure (21) Projectile CG Jump Summary

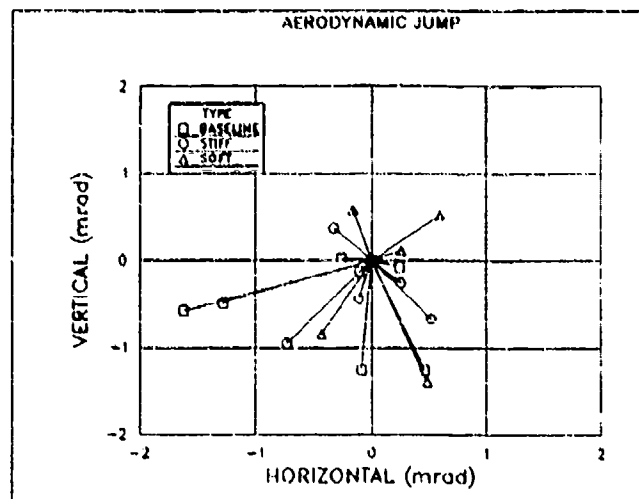


Figure (22) Aerodynamic Jump Summary

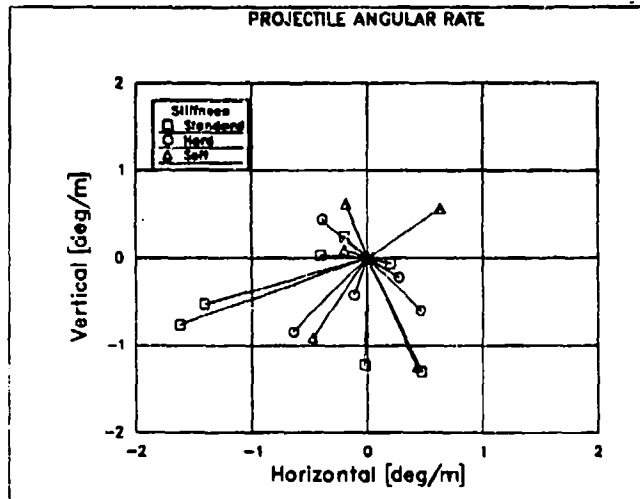


Figure (23) Projectile Angular Rate at the Muzzle

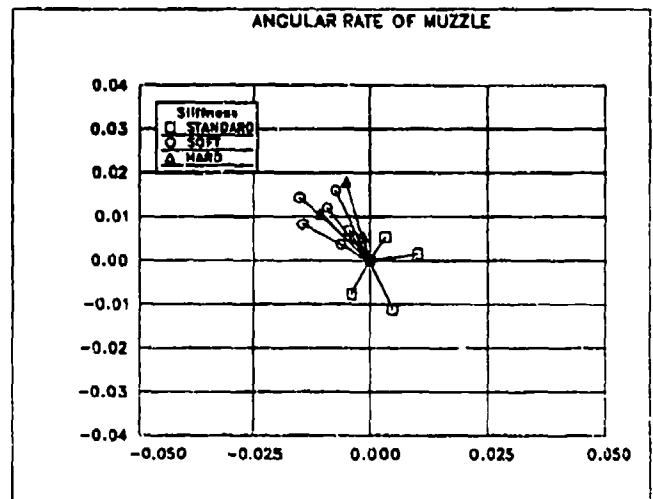


Figure (24) Gun Muzzle Angular Rate

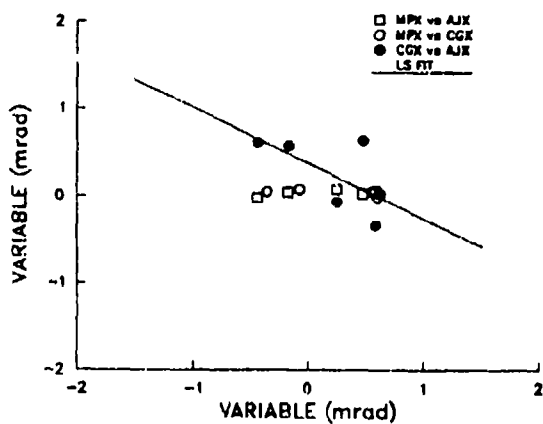


Figure (25) Cross Correlations for the Soft Configuration

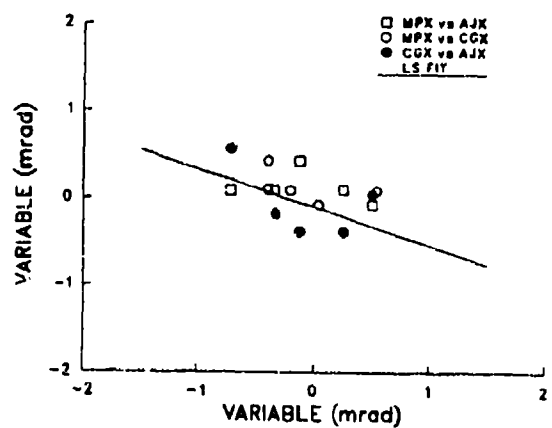


Figure (26) Cross Correlations for the Stiff Configuration

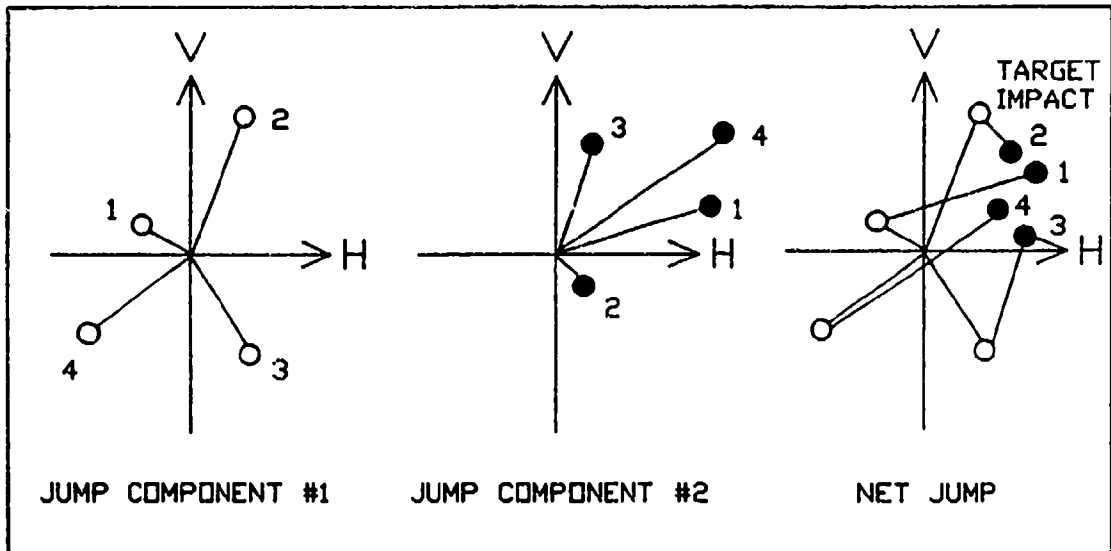


Figure (27) Jump Correlation Effect Schematic

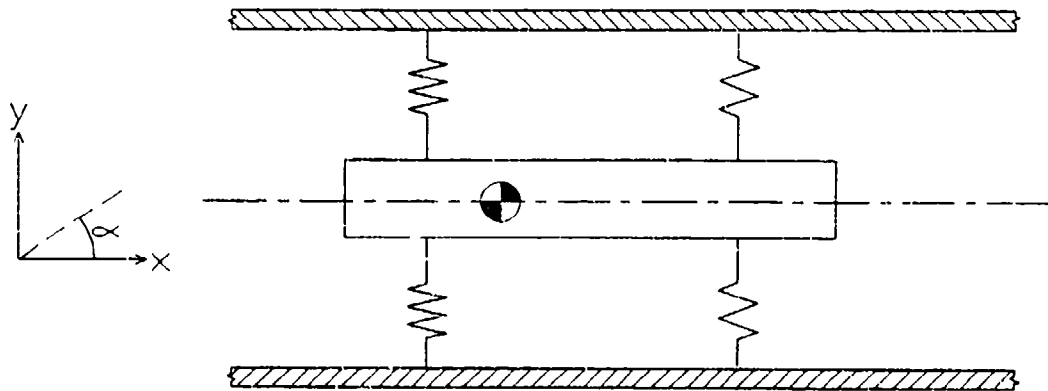


Figure (28) Geometry for the problem of a rigid beam supported by four springs

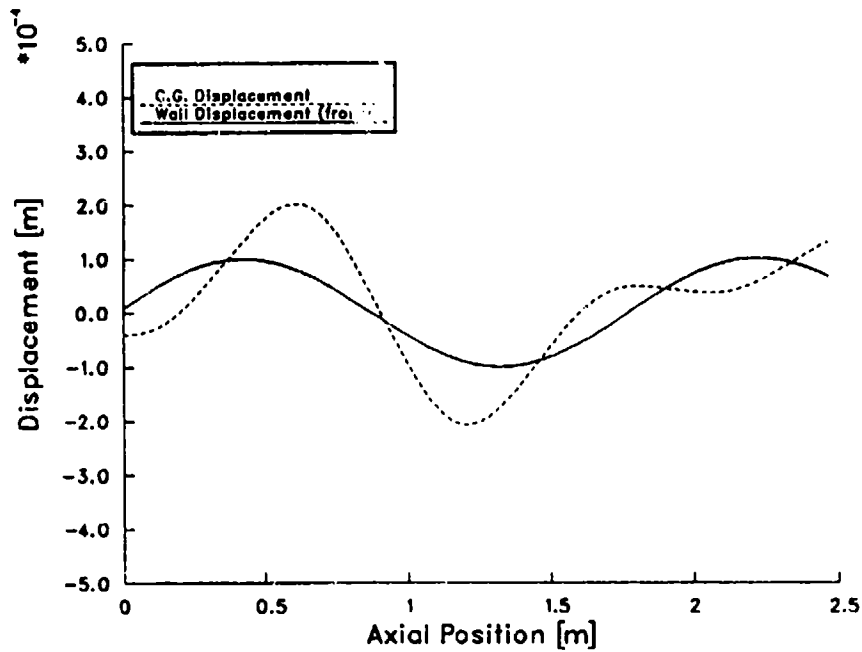


Figure (29) Linear displacement of rod center of gravity when traversing a guntube with a sinusoidal bore centerline

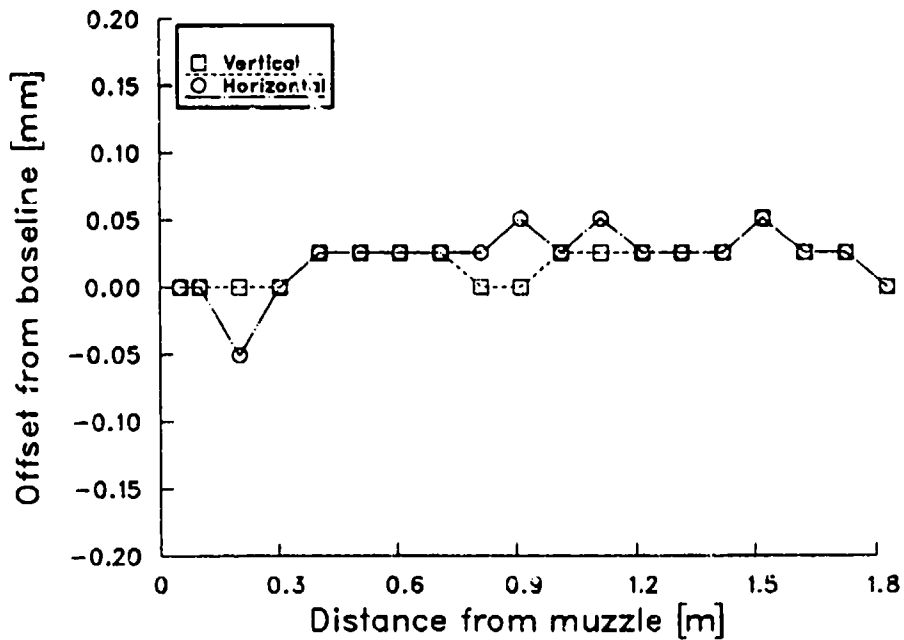


Figure (30) Bore centerline profile for 25mm Mann barrel used in the test

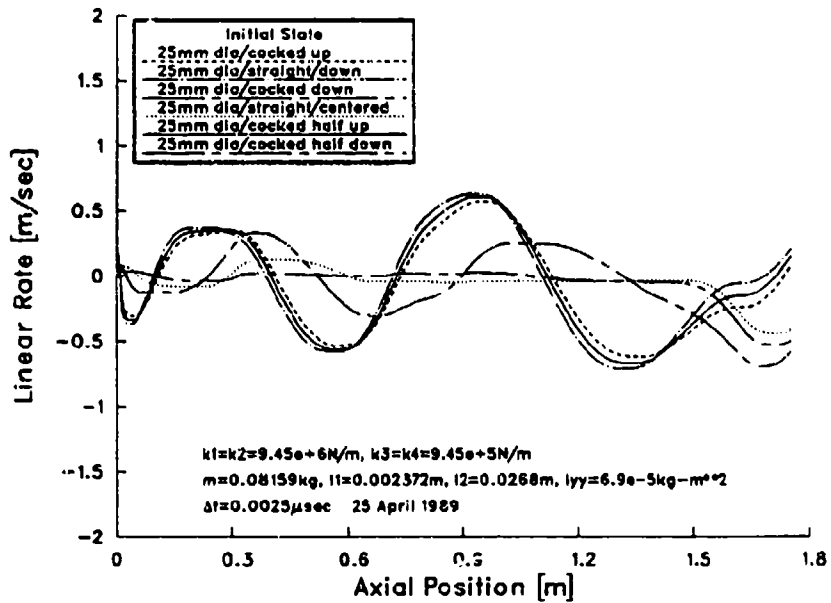


Figure (31) Linear velocity of the rod center of gravity perpendicular to the centerline of the gun tube

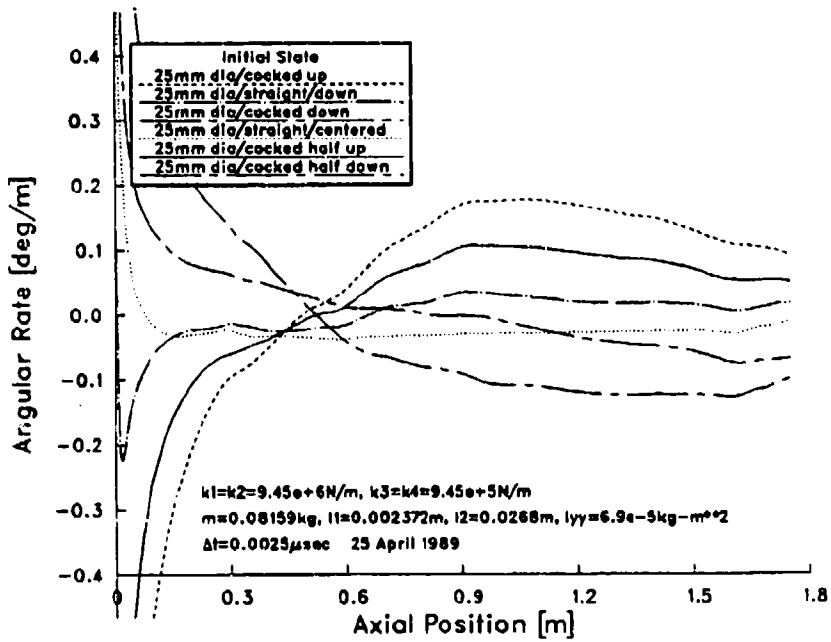


Figure (32) Angular rate of the rod

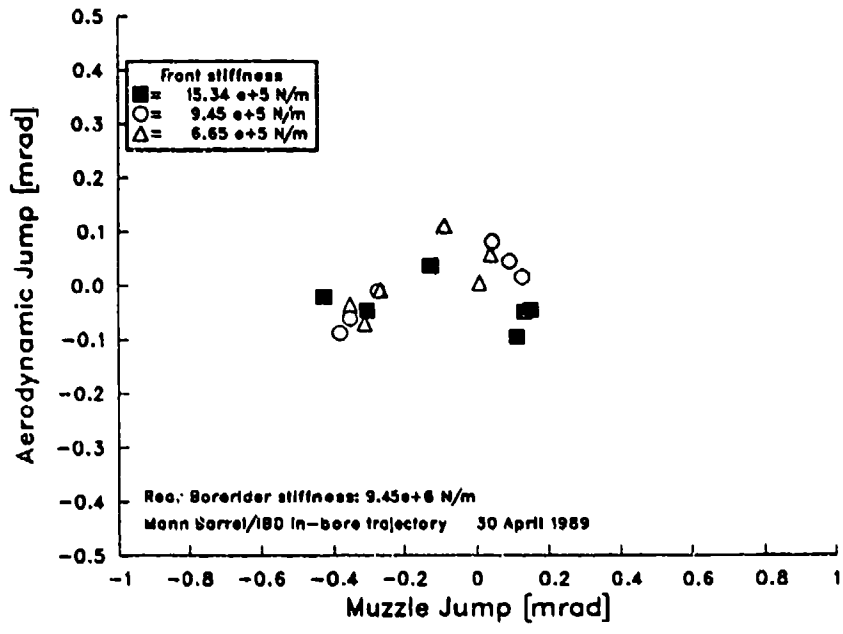


Figure (33) Correlation between aerodynamic and linear jump at the muzzle, in the vertical plane

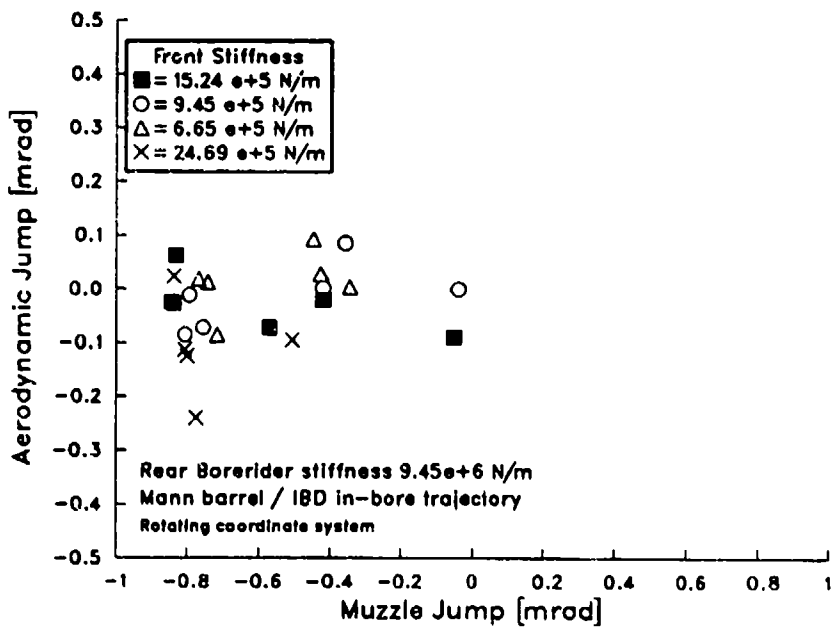


Figure (34) Correlation between aerodynamic and linear jump at the muzzle for a rotating coordinate system

Configuration	Stiffness (nt/m)	% of Baseline
Baseline	9.45×10^5	100
Stiff	15.24×10^5	161
Soft	6.65×10^5	71

Table (1) Front Borerider Stiffness

Configuration	X_{mean}	Y_{mean}	σ_x	σ_y
Baseline	-0.467	-0.187	0.83	0.60
Stiff	-0.055	-0.10	0.32	0.40
Soft	0.44	0.01	0.39	0.94

Table (2) Measured Target Impact Dispersion

Component	X_{mean}	Y_{mean}	σ_x	σ_y	σ_x^2	σ_y^2
Muzzle Pointing Angle	0.140	0.040	0.17	0.09	0.0289	0.0081
Muzzle Crossing Velocity	-0.007	-0.004	0.02	0.02	0.0004	0.0004
Projectile CG Jump	-0.210	0.480	0.27	0.20	0.0729	0.0400
Aerodynamic Jump	-0.380	-0.540	0.78	0.58	0.6084	0.2916
Sum	-0.457	-0.049	0.85	0.58	0.7106	0.3401
Measured	-0.467	-0.187	0.83	0.60	0.6889	0.3600

Table (3) Mean Impact and Dispersion Summary - Baseline Configuration

Component	X_{mean}	Y_{mean}	σ_x	σ_y	σ_x^2	σ_y^2
Muzzle Pointing Angle	0.120	-0.180	0.18	0.17	0.0324	0.0289
Muzzle Crossing Velocity	-0.020	0.003	0.01	0.01	0.0001	0.0001
Projectile CG Jump	-0.074	0.607	0.40	0.34	0.1600	0.1156
Aerodynamic Jump	-0.080	-0.390	0.49	0.50	0.2401	0.2500
Sum	-0.054	0.040	0.65	0.63	0.4326	0.3946
Measured	-0.055	-0.100	0.32	0.40	0.1024	0.1600

Table (4) Mean Impact and Dispersion Summary - Stiff Configuration

Component	X_{mean}	Y_{mean}	σ_x	σ_y	σ_x^2	σ_y^2
Muzzle Pointing Angle	0.03	-0.11	0.040	0.150	0.0016	0.0225
Muzzle Crossing Velocity	-0.02	-0.00	0.013	0.029	0.0002	0.0008
Projectile CG Jump	0.28	0.43	0.450	0.190	0.2025	0.0361
Aerodynamic Jump	0.15	-0.20	0.430	0.870	0.1849	0.7569
Sum	0.44	0.12	0.620	0.900	0.3892	0.8163
Measured	0.44	0.01	0.390	0.940	0.1521	0.8836

Table (5) Mean Impact and Dispersion Summary - Soft Configuration

Component Description	Term Eqn. (3)	Stiff		Soft	
		Horizontal	Vertical	Horizontal	Vertical
Muzzle Pointing Angle	σ_{mp}^2	0.0324	0.0289	0.0016	0.0225
Muzzle Crossing Velocity	σ_{cv}^2	0.0001	0.0001	0.0002	0.0008
Projectile CG Jump	σ_{cg}^2	0.1600	0.1156	0.2025	0.0361
Aerodynamic Jump	σ_{aj}^2	0.2401	0.2500	0.1849	0.7569
Correlation	$2\sigma_{cgaaj}$	-0.2040	-0.1518	-0.2380	0.0000
Sum Eqn. (3)	σ^2	0.2286	0.2428	0.1512	0.8136
Measured	σ^2	0.1024	0.1600	0.1521	0.8836
Sum Eqn. (3)	σ	0.48	0.49	0.39	0.90
Measured	σ	0.32	0.40	0.39	0.94

Table (6) Dispersion Results with Jump Correlation Terms

References

1. Haug, B.T. & Bornstein, J.A., "Gun Dynamics Measurements for Tank Gun Systems," in the Proceedings of the Fifth U.S. Army Symposium on Gun Dynamics, T.E. Simkins & Clarke G. Homan eds., U.S. Army ARDEC, Benet Laboratories, Attn: SMCAR-CCB-TL, Watervliet, NY 12189, 1987
2. Schmidt, E.M., Plostins, P. & Bundy, M.L., "Flash Radiographic Diagnostics of Projectile Launch," in the Proceedings of the 1984 Flash Radiographic Symposium, E.A. Webster, Jr. & A.M Kennedy eds., The American Society for Nondestructive Testing, 4135 Arlingate Plaze, Columbus, OH, 43221, 1984
3. Plostins, P. & White, C.O., "The Transitional Ballistics, Aeroballistics and Jump Characteristics of a 25mm-AP Training Projectile with Base Bleed," in the Proceedings of the Tenth International Symposium on Ballistics, American Defense Preparedness Association, 1987
4. Murphy, C.H., "Free Flight Motion of Symmetric Missiles," BRL Technical Report 1216, U.S. Army Ballistics Research Laboratory, Aberdeen Proving Ground, MD 21005, 1963, AD 442757
5. Gay, H.P. & Elder, A.S., "The Lateral Motion of a Tank Gun and its Effect on the Accuracy of Fire," Ballistics Research Lab Report 1070, U.S. Army Ballistics Research Laboratory, Aberdeen Proving Ground, MD, 21005, 1959, AD 217657
6. Biele, J.K., "The Relationship of Gun Dynamics to Accuracy in a 120mm Tank Gun," in the Proceedings of the 8th International Symposium on Ballistics, American Defense Preparedness Association, 1984
7. Plostins, P., "Launch Dynamics of APFSDS Ammunition," Technical Report BRL-TR-2595, U.S. Army Ballistics Research Laboratory, Aberdeen Proving Ground, MD 21005, 1984, AD A147374
8. Ott, L., "An Introduction to Statistical Methods and Data Analysis," Duxbury Press, Boston, 1984
9. Erline, T.F. & Kregel, M.D., "RASCAL, A 2-D Gun Dynamics Program," BRL Technical Report, to be published
10. Soifer, M.T. & Becker, R.S., "Dynamic Analysis of the 75mm ADMAG Gun System," BRL Contractor Report USABRL-CR-495, December 1982, AD A1238671
11. Raybern, D.A., "Axially Accelerated Saboted Rods Subjected to Lateral Forces," Report LA-11494-MS, Los Alamos National Laboratory, Los Alamos, NM 87545, March 1989

12. Kreyszig, E., "Advanced Engineering Mathematics," John Wiley & Son, New York, 1972, p. 670
13. Baer, P.G. & Frankle, J.M., "The Simulation of Interior Ballistic Performance of Guns by Digital Computer Program," BRL Report 1183, Ballistic Research Lab, Aberdeen Proving Ground, MD 21005, 1962, AD 299980

BRL MANDATORY DISTRIBUTION LIST

<u>No of</u> <u>Copies</u>	<u>Organization</u>	<u>No of</u> <u>Copies</u>	<u>Organization</u>
(Unclass., unlimited) 12	Administrator	1	Commander
(Unclass., limited) 2	Defense Technical Info Center		US Army Missile Command
(Classified) 2	ATTN: DTIC-DDA Cameron Station Alexandria, VA 22304-6145		ATTN: AMSMI-RD-CS-R (DOC) Redstone Arsenal, AL 35898-5010
1	HQDA (SARD-TR) WASH, DC 20310-0001	1	Commander US Army Tank Automotive Command ATTN: AMSTA-TSL (Technical Library) Warren, MI 48397-5000
1	Commander US Army Materiel Command ATTN: AMCDRA-ST 5001 Eisenhower Avenue Alexandria, VA 22333-0001	1	Director US Army TRADOC Analysis Command ATTN: ATAA-SL White Sands Missile Range, NM 88002-5502
1	Commander US Army Laboratory Command ATTN: AMSLC-DL Adelphi, MD 20783-1145	(Class. only) 1	Commandant US Army Infantry School ATTN: ATSH-CD (Security Mgr.) Fort Benning, GA 31905-5660
2	Commander Armament RD&E Center US Army AMCCOM ATTN: SMCAR-MSI Picatinny Arsenal, NJ 07806-5000	(Unclass. only) 1	Commandant US Army Infantry School ATTN: ATSH-CD-CSO-OR Fort Benning, GA 31905-5660
2	Commander Armament RD&E Center US Army AMCCOM ATTN: SMCAR-TDC Picatinny Arsenal, NJ 07806-5000	1	The Rand Corporation P.O. Box 2138 Santa Monica, CA 90401-2138
1	Director Benet Weapons Laboratory Armament RD&E Center US Army AMCCOM ATTN: SMCAR-LCB-TL Watervliet, NY 12189-4050	(Class. only) 1	Air Force Armament Laboratory ATTN: AFATL/DLODL Eglin AFB, FL 32542-5000
1	Commander US Army Armament, Munitions and Chemical Command ATTN: SMCAR-ESP-L Rock Island, IL 61299-5000		<u>Aberdeen Proving Ground</u> Dir, USAMSAA ATTN: AMXSY-D AMXSY-MP, H. Cohen Cdr, USATECOM ATTN: AMSTE-TO-F Cdr, CRDEC, AMCCOM ATTN: SMCCR-RSP-A SMCCR-MU SMCCR-MSI
1	Commander US Army Aviation Systems Command ATTN: AMSAV-DACL 4300 Goodfellow Blvd. St. Louis, MO 63120-1798		
1	Director US Army Aviation Research and Technology Activity Ames Research Center Moffett Field, CA 94035-1099		

DISTRIBUTION LIST

<u>No. of Copies</u>	<u>Organization</u>	<u>No. of Copies</u>	<u>Organization</u>
11	<p>Commander Armament RD&E Center US Army AMCCOM ATTN:SMCAR-CCL-CA</p> <p>P. O'Neill C. A. Miller E. Malatesta R. Cirkurs J. Hirlinger G. Fleming</p> <p>SMCAR-CCL-CH SMCAR-CCH-V</p> <p>SMCAR-AEI-A</p> <p>Dover, NJ 07801-5001</p>	2	<p>Director Benet Weapons Laboratory ATTN: SMCAR-CCB, L. Johnson T. Simkins Watervliet, NY 12189</p>
		1	<p>Commander US Army Armor Center & School ATTN: ATSB-SMT, Maj Newlin Fort Knox, KY 40121</p>
		2	<p>Olin Corporation ATTN: L.A. Mason D. Marlowe 707 Berkshire Blvd East Alton, IL 62024</p>
2	<p>President US Army Armor & Engineer Board ATTN: AT2K-AE-PD, Fort Knox, KY 40121</p> <p>Mr. A. Pomey Mr. W. Wells</p>	4	<p>Honeywell, Inc. 600 Second Street, NE ATTN: C. Rippe R. Becker C. Candland G. Stilley Hopkins, MN 55343</p>
6	<p>Commander US Army Tank Automotive Command ATTN:PM-M1A1, LTC Barbara LTC Kaye Mr. G. Howe Dr. M. Pattison</p> <p>ATTN:PM-M1 ATTN:PM-M60 Warren, MI 48090</p>	1	<p>Honeywell Inc ATTN: D. Magnes 7225 Northland Drive Brooklyn Park, MN 55428</p>
		1	<p>Honeywell Inc ATTN: R. Gartner 10400 Yellow Circle Drive Minnetonka, MN 55343</p>
4	<p>Commander Tank Main Armament Systems ATTN: AMCPM-TMA, R. Billington K. Russell V. Rosamillia E. Kopacz</p> <p>Dover, NJ 07801-5001</p>	4	<p>Aerojet Ordnance Co ATTN: W. Wolterman S. Rush J. Parkinson D. LaFevre 2521 Michelle Drive Tustin, CA 92680</p>

DISTRIBUTION LIST

<u>No. of Copies</u>	<u>Organization</u>
2	Arrow Tech Associates, Inc ATTN: B. Whyte W. Hathaway P.O. Box 4218 South Burlington, VT 05401-0042
1	AAI Corporation ATTN: J. Herbert P.O. Box 6767 Baltimore MD 21204
1	Los Alamos National Laboratory ATTN: Dr. D.A. Rabern P.O. Box 1663 (WX-4, Mail C-787) Los Alamos, NM 87545
1	Battelle Pacific Northwest Laboratory ATTN: Mr. J. E. Diebler Engineering Physics Department Battelle Boulevard Richland, WA 99352

Aberdeen Proving Ground

Director, USAMSAA
ATTN: AMXS-D, Mr. W. Brooks
Mr. B. Siegel
Mr. R. Conroy

Commander, USACSTA
ATTN: STECS-AV-T, Mr. W. Swank
ATTN: STECS-AS-HT, Mr. H. Zelik
Mr. H. Greuter

Commander, USATECOM
ATTN: AMSTE-TE-R, Mr. Keele
ATTN: AMSTE-CM-R, Mr. Saubier

USER EVALUATION SHEET/CHANGE OF ADDRESS

This laboratory undertakes a continuing effort to improve the quality of the reports it publishes. Your comments/answers below will aid us in our efforts.

- 1. Does this report satisfy a need? (Comment on purpose, related project, or other area of interest for which the report will be used.) _____

- 2. How, specifically, is the report being used? (Information source, design data, procedure, source of ideas, etc.) _____

- 3. Has the information in this report led to any quantitative savings as far as man-hours or dollars saved, operating costs avoided, or efficiencies achieved, etc? If so, please elaborate. _____

- 4. General Comments. What do you think should be changed to improve future reports? (Indicate changes to organization, technical content, format, etc.) _____

BRL Report Number _____ Division Symbol _____

Check here if desire to be removed from distribution list. _____

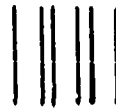
Check here for address change. _____

Current address: Organization _____
Address _____

-----FOLD AND TAPE CLOSED-----

Director
U.S. Army Ballistic Research Laboratory
ATTN: SLCBR-DD-T (NEI)
Aberdeen Proving Ground, MD 21005-5066

OFFICIAL BUSINESS



NO POSTAGE
NECESSARY
IF MAILED
IN THE
UNITED STATES

BUSINESS REPLY LABEL
FIRST CLASS PERMIT NO 12062 WASHINGTON D C

POSTAGE WILL BE PAID BY DEPARTMENT OF THE ARMY



Director
U.S. Army Ballistic Research Laboratory
ATTN: SLCBR-DD-T (NEI)
Aberdeen Proving Ground, MD 21005-9989